International Journal of Multidisciplinary Approach and Studies

ISSN NO:: 2348 – 537X

# A generic approach for human lungs CT scan Image analysis using Deep learning technique

**Dr. M. Mohamed Sathik* & S Piramu Kailasam****

****Principal,Sadakathullah Appa College,Tirunelveli,India ,*
*****Assistant Professor,Sadakathullah Appa College,Tirunelveli,India,*

**ABSTRACT:**

*The lower part of the human lungs (HL) has increased, in which many unknown events are coming. In complex tuberculosis, restoration of hanging in lungs, prevent further complications and eliminate bacteria. Complex Neck Run Management is still controversial, and surgery is one of the cures that should be estimated according to its role in treating complicated illness. This study is a case-based case report. The database used for finding literature is cocaine, medical and proposal. The main word Primary lungs ninety runner, surgery, pulmonary ambulance and baby search. The quality added is , under 18 years of children. As per the diagnosis of 2019, according to evidence, Arthy Centre was organized according to Medical to Medicine. Six joint studies have been analyzed. Surgery was diagnosed for surgical patients, who did not respond to the treatment. It should be noted that standard DLT-WOO,CBX,CMC dataset is tested before using and therefore it may differ from existing usage. At the same time, We go into the lungs Acquisition after acquisition we become one 96.77% accuracy Deep learning technique (DLT Method) there are instructions suhisen algorithm using on lung prevention. However, compared with surgery, with lower part of the complicated lungs there is better death and patient among children.*

**Keywords -** *lungs, surgery, treatment, patient,Sushisen algorithms,DLT*

## INTRODUCTION

The analysis 9.6 million new cases and 1.5 million deaths were reported in tuberculosis (TB). Of the new cases, there are 1 million child cases. The prevalence of pulmonary tuberculosis in children is on the rise, and many cases remain. [1] Early oral therapy was the best predictor of childhood tuberculosis, however, due to prolonged treatment, incomplete treatment, relapse, and increased risk of complications.

Treatment of complex lung tuberculosis was not limited to bacterial eradication, but to return to normal lung function and prevent further complications. Recovery surgery with physical abnormalities in 3,4 complex tuberculosis patients with functional disruption and antitubercularis. Recovery surgery is the only treatment for pulmonary tuberculosis in children with permanent bronchial destruction. By combining oral therapy and surgery with the right type and timing of surgery, complications can be stopped and lung function recovered.

**Review of Literature**

**CASE DLT METHODS ILLUSTRATION IN SIFT**

Main complaint was two months ago, came to the emergency room with a 9-month-old boy five months ago. Producer cough, fever and hunger. Pulmonary tuberculosis had a family history. Six months before the hospital admission, the patient had a standard dose combination (FTC) regimen (30 mg isoniazid, 60 mg rifampicin, and 150 mg pyrazinide) in the midst of oral antiaridulosis therapy.

There is no history of the Bacillus Calamite Guerin (PCG) vaccine. By physical examination, the child suffered from malnutrition, failed to develop and was stable hemodynamic. Dyspnea was observed using sternocleidomastoid muscles and intercostyle muscles. From the chest rhythm, the upper left breast was hypercaricular, and vesicular breathing sounds were observed with the bilateral roach.

With laboratory use, leukocyte 28.230 / cL, c-reactive protein (CRP) 10,4 mg / L, procoalkidone 3,4 ng / ml, erythrocyte sedimentation rate 5 mm. Acid-fast stains showed negative results from sputum. Tuberculosis testing was positive. X-ray of the aperture and lateral chest shows eradication in the ventricle, which shows the upper right lung. The results of the CT scan showed multiple cystic lesions with varying sizes, including the largest lesion being 7.13 cm in diameter, where the pulmonary tuberculosis cavity in both lungs was compressed in all lobes.

**STRUCTURE OF THE PAPER**

Next Section deals with the detailed architecture listing all the involved steps viz. pre-processing of CT images, features and classifier details. In Section 3, we will talk about the datasets used for training , validation and testing of the classification models. Results, Conclusion and Future scope are described in Section 4 and 5 respectively. Section 6 is for acknowledgements.

International Journal of Multidisciplinary Approach and Studies
ISSN NO:: 2348 – 537X

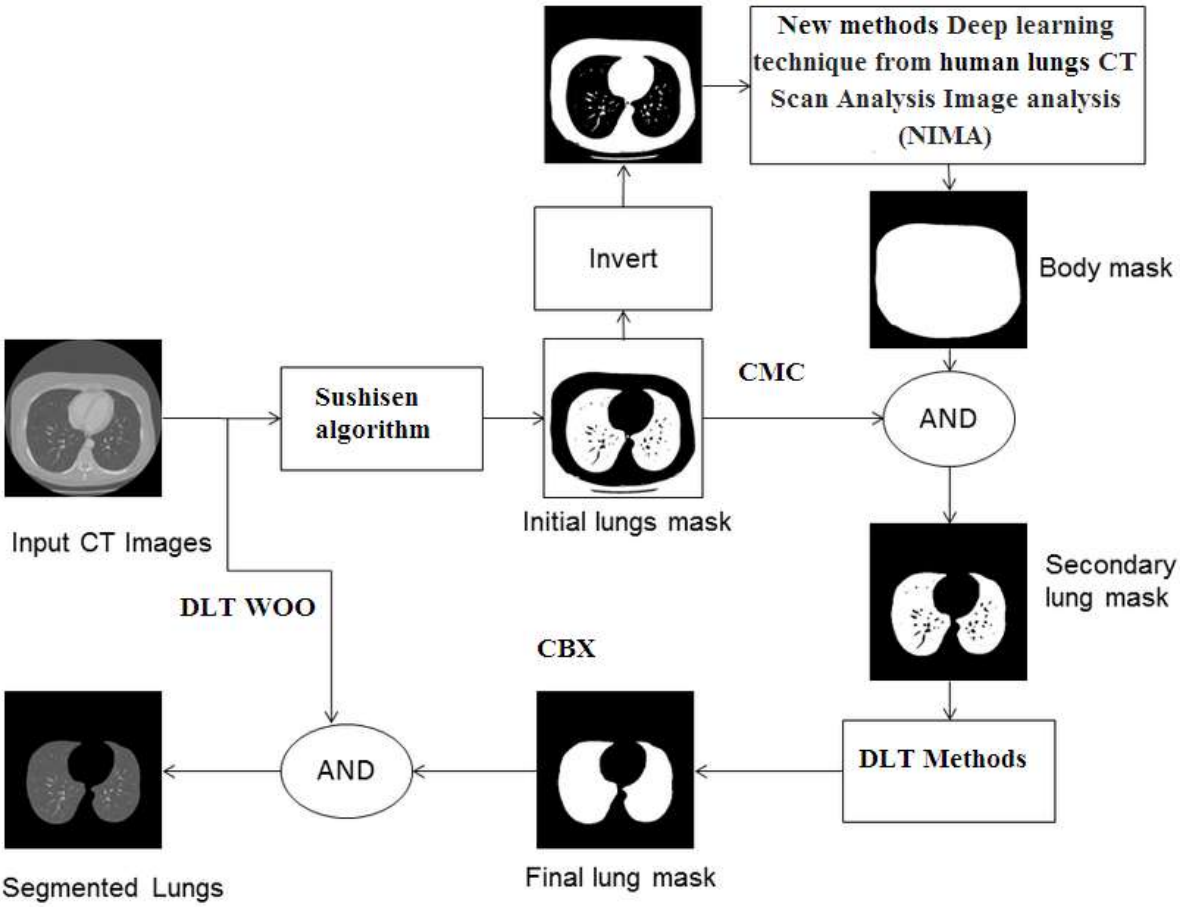


Fig 1 : The proposed training loop with adaptive sampling of the training images

**Sushisen Algorithm**

**Input: Metric Start = I, start with the identity matrix.**

**Spread the nearest neighbor of KM points around the test point xo in Σ metric read.**

**Calculate the weight between classes and matrices between W and B using the Ices and TSS (T = W + B) points.**

**Define the new metric W = W-1/2 [W-1 / 2BW-1/2 + -I] W-1/2**

**. Output: Segementation after classification at Test Point x accuracy 97..**

1. DLT Methods Regression: Y = a + b X.
A. Two parameters A and B indicate the curve and are estimated using the data at hand.
B. Use the least square parameters for known values of Y1, Y2, ..., X1, X2.
2.DLT Regression: Y = b0 + b1 x1 + b2 x2.
3. DTL. (Dataset) = truncate (tree_generation (dataset))
4. knn.tree_generation (dataset) = if finish_discount (dataset)
5. Address (majority_category (dataset))
6. Training Data Form (X1, Y1), (X2, Y2),,, (X | | |, Y | D |)
7. Examining 2-D data, we may have: y = w0 + w1 x1 + w2 x2
Otherwise .. do (test. Training = 100%)
9. Best_Test = FE_Function (Dataset)
10. On the node

11. Training Data: Error_ Training (h)
12. Full Distribution of Data D: Error_D (h)
13. Suhisen (error_ training (h) <error_ training (h))
14. error_D (h)> error (h ')
15. For every value of the besttest
16. Subtree_V = Tree_Generation ({e Example; eBest_Test = V)
17. In the (best_test, subtree_v) node
18. Comparison NB = Best. Breed + test;
19. The result of accuracy;

**NIMA FLOW CHAT**

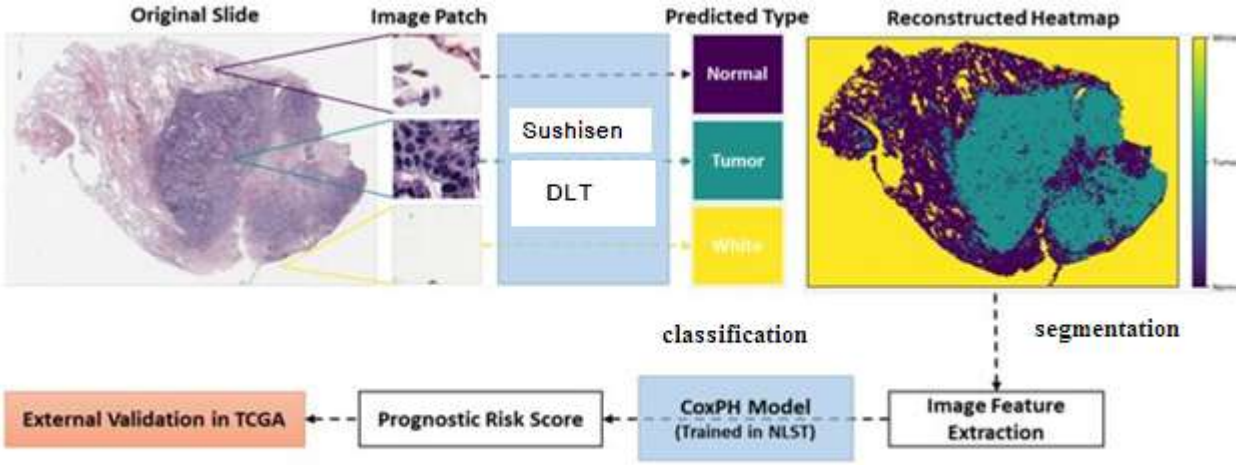


Fig 2: Flow chart of NIMA

**METHODOLOGY**

All evaluation studies were studied in conjunction with the patients, until the outcome was not available until treatment. There were 13 low-level 4 because there was no control group in the joint study, least sample computation and no statistically significant analysis.

The only study that directly compared the effects of morbidity and mortality on surgical and antidepressant medications, Darton et al. Therefore, it is possible to fully evaluate the validity parameters using these studies. The surgery was performed on the basis of 8 symptoms, there was no anomaly, and there was variability in the patient's original characteristics, including the occurrence of acute illness. Antibiotics were usually administered only to treatment groups. There was no statistical analysis or blindness, but the objective outcome (mortality and morbidity) prevented measurement bias.

**a) Predicted Type**:

Significance can be measured by the required number of treatments (NNT), with the NNT of the study being 15.89 or 16.12 targets. For 16 lobectomy, 1 flap or persistent bronchitis can be prevented. Despite good validity, the study should be used with caution. A study in Liverpool, completed in 1957, compared to Indonesia, found that antibiotic drugs were not

validated with different sociology and ethnicities. The problem found in the study is also different from the case

Other literature did not evaluate the control group and, therefore, could not assess the validity. One aspect of computational imports is the test incidence rate (EER), which defines the ratio of patients with outcomes compared to total subjects. For mortality, ERR ranged from 0 to 13%, and the incidence of illness was 0 to 38%.

**b) Reconstruct Map**

Primary tuberculosis after early infection of MDP. In children, mature tuberculosis can lead to bronchial obstruction and ventricular dysfunction. 15 complications can cause breathing difficulties, so the decision to undergo surgery or conventional therapy should be addressed. There was no guidance in decision making, which created controversy about the patient's eligibility and when to perform 15 surgeries

Validity defines the validity of the study. Cameron et al have not shown the underlying characteristic of the subjects and the treatment objective of the analysis. There may be deceptive factors that affect the outcome of the study. [13] Surgery cannot be blinded to treatment, so there must be an objective reduction in the dependence effect. From the 13 major analyzes of the literature, there are many points to note.

**c) Segmentation of feature extraction**

1. Includes multiple holes> 1 flap
2. The large cavity consists of> 2 adjacent folds
3. The large cavity contains a significant paranoid ulcer and is unable to partially implant
4. Pores with signs of knot disease
5. Major tracheal branch stenosis

**d) Classification of coxPH model**

1. Unilateral pits are limited to a specific area where there is no improvement after conservative treatment
2. Increase the pressure in the cavities
3. Diagnosis, secondary to bronchitis, cavity and endopranchial obstruction

In addition, other signs of surgery include:

1. The case of immunity towards conservative treatment
2. Lung of advanced and irreversible chronic fibroids

Antide pressolysis was performed postoperatively to reduce disease activity and proved to be a good outcome in surgery. Careful selection was necessary to treat lung tuberculosis patients. Cameron et al found that 31 patients who were injured in the non-surgical section had not been reactivated, concluding that surgery was not recommended to prevent complications.

Mortality was higher among surgical patients, but the baseline characteristics of the groups were different and patients in poor condition underwent surgery. On the other hand, comparisons of efficacy of surgery and conventional therapy for children with complex lung tuberculosis are unethical.

**e) Prognotic Risk score**

In this case, the patient had many symptoms, such as an unresponsive small child and an anatomical ulcer that showed chest x-ray and CT scan. It called for surgical evaluation with six review literature

$$\hat{k} = \frac{N\sum_{i=1}^{r} x_{ii} - \sum_{i=1}^{r}(x_{i+} \cdot x_{+i})}{N^2 - \sum_{i=1}^{r}(x_{i+} \cdot x_{+i})}$$

$$\sum_{i=1}^{r} x_{ii} = 226+216+360+397+190+219 = 1608$$

$$\sum_{i=1}^{r} x_{ii} = 226+216+360+397+190+219 = 1608$$

$$\hat{k} = \frac{2480 \times 1608 - 1{,}124{,}382}{2480^2 - 1{,}124{,}382} = 0.9677$$

**IMPLEMENTATION**

**a)Data Set**

This analysis for the three datasets (DLT-WOO,CMC,CMC) used by us Dataset made available by the National Library Science. 326 with normal cases and 336 with its 662 pictures. Tuberculosis cancer case With each CXR image, a brief report This includes the patient's age, gender and diagnosis. All X-ray images are not the same size, but 3K X 3K can be better. Around. Second dataset is Indian Dataset This CMC works for Vellore. There are 56 common cases In the .jpg format, 70 cases of tuberculosis have been given. The resolution of images varies from 1.5K to 1.5K to 2.7k.

**b) Computation phase**

(1) We use the algorithm in to calculate X-ray image of the model. This pattern produces a Maps are probably more similar sets and then defines transforming mapping original patient's X-ray image registration.

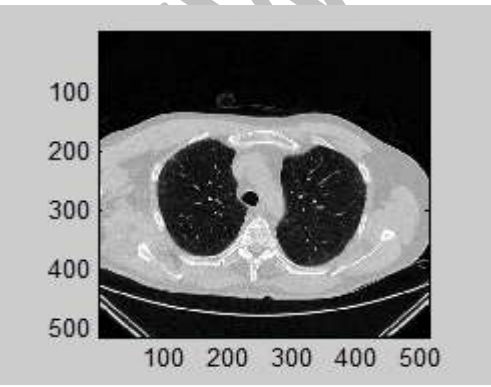


| Type | **Features DLT WOO Data** | **Features CMC,CBX** | **Proposed Features New Method** |
|---|---|---|---|
| Sushisen | 85.5 | 88.25 | 96.77 |
| DLT | 82.5.5 | 85.46 | 88.84 |

Fig3:(a) data set segmentation Phase CMC image (b) Result CMC dataset NIMA value

(2) The rib map is doubled further along the range of 0.5 950 (this value) with all the connected components Dataset needs to be modified based on pixels Removed to get cleaner rib map It is being done Further calculation in any false margin.

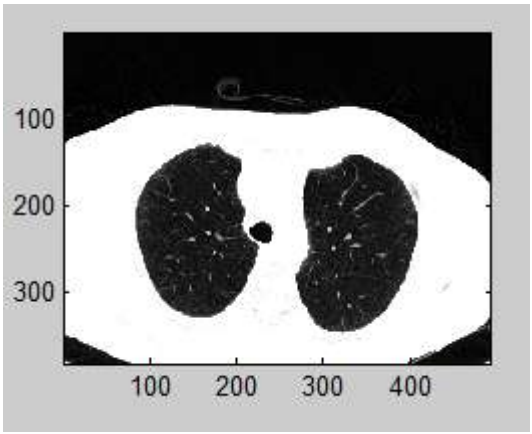


| Type | **Features DLT WOO Data** | **Features CMC,CBX** | **Proposed Features New Method** |
|---|---|---|---|
| Sushisen | 85.5 | 88.25 | 96.33 |
| DLT | 82.5.5 | 85.46 | 78.84 |

Fig :4 (a) data set segmentation CBX image (b) Result CBX dataset NIMA value

(3) Around the area that detects the costphronic angle Only 20% of the area's two lungs are considered For further calculation. This percentage should be of the value Tune in based on your data-set.

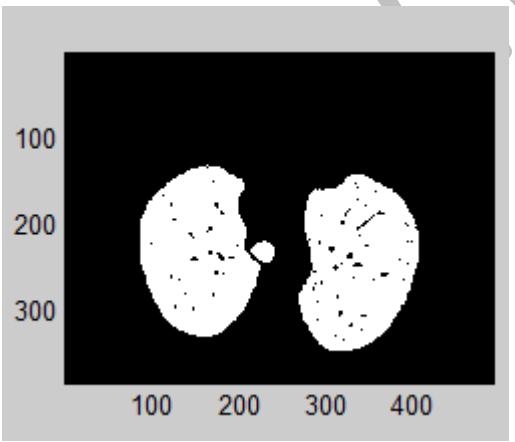


| Type | **Features DLT WOO Data** | **Features CMC,CBX** | **Proposed Features New Method** |
|---|---|---|---|
| Sushisen | 81.5 | 78.25 | 92.77 |
| DLT | 82.5 | 82.16 | 78.24 |

Fig 5: (a) data set DLT-WOO segmentation image (b) Result DLT-DOO NIMA value

(4) For the revised image, we have calculated indexed points the last non-zero points are the lungs of the costoffrenic angle For each column of the image.

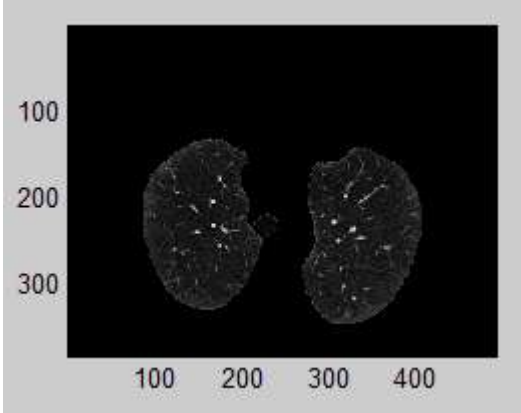


(a) Real dataset result

| Type | Features DLT WOO Data | Features CMC,CBX | Proposed Features New Method |
|---|---|---|---|
| Sushisen | 81.5 | 78.25 | 92.77 |
| DLT | 82.5 | 82.16 | 78.24 |

(b) real data set results

(5) Using a binary rib map of gradient computed is a sobel Operator To avoid any fraudulent calculations At the end of the lung, the interval is not the same), we only remove In the 20% internal area, calculate high for each lung.

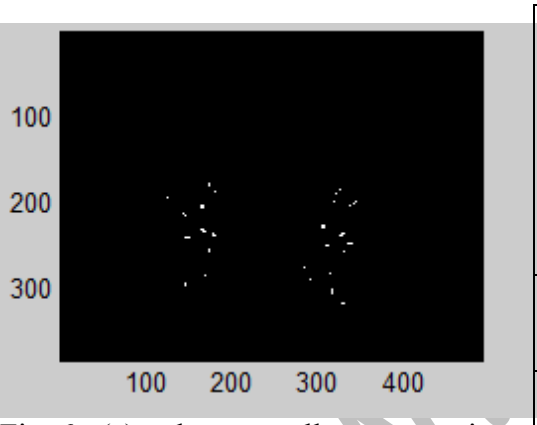


Fig 6: (a) data set all segmentation image

| Type | Features DLT WOO Data | Features CMC,CBX | Proposed Features New Method |
|---|---|---|---|
| Sushisen | 85.5 | 88.25 | 96.77 |
| DLT | 82.5.5 | 85.46 | 88.84 |

(b) Result all NIMA value

**RESULT**

Study is an Evidence-Based Case Report. Medline, Proquest, and Cynadirect are synonyms have been added in a wide range of search results, including "lungs", "operation" and "hair disease". literature search, six articles were selected and then withdrawn in Table 1. Most of the studies were done before the era of many antituberbularis regimens. Primary tuberculosis surgery after standard treatment with leptocycin (Strape) and para-aminosalicylic examined 48 cases of pulmonary TB in children with segmental lesion complications from 2015 to 2019. Based on the results of bronchoscopy after adequate oral therapy, five patients were rescued. The traditional treatment group was not given antibiotics, but was rested in bed and was observed intensely in the ward. Reported 101 cases of pulmonary tuberculosis in children. Primary tuberculosis complications were present in 69,3% of cases. 9 Feltis and Campbell reported a potential colleague, who had undergone surgery with 47 children with pulmonary tuberculosis. A study by surgery, persistent cavity, fibonodular disease, atllectasis,

and lost lung / lobe 10 quinlan et al. Cavity, bronchiectasis, waste lung / lobe and middle ear syndrome.

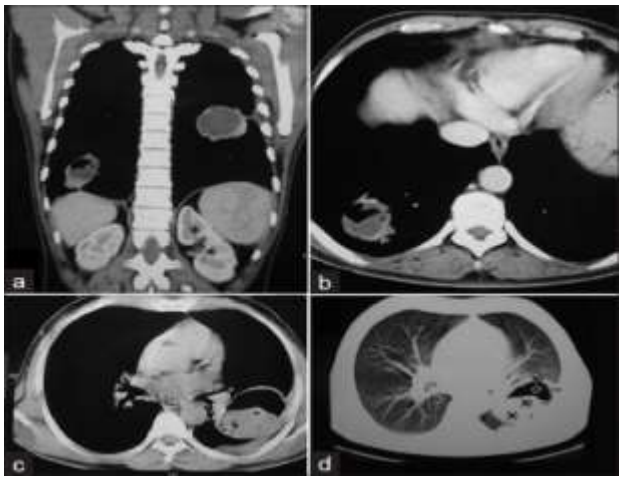


(a)

(b)

Fig: 7 (a) segmentation uncertainty map computed using the proposed method, (b) the same for Platt scaling method

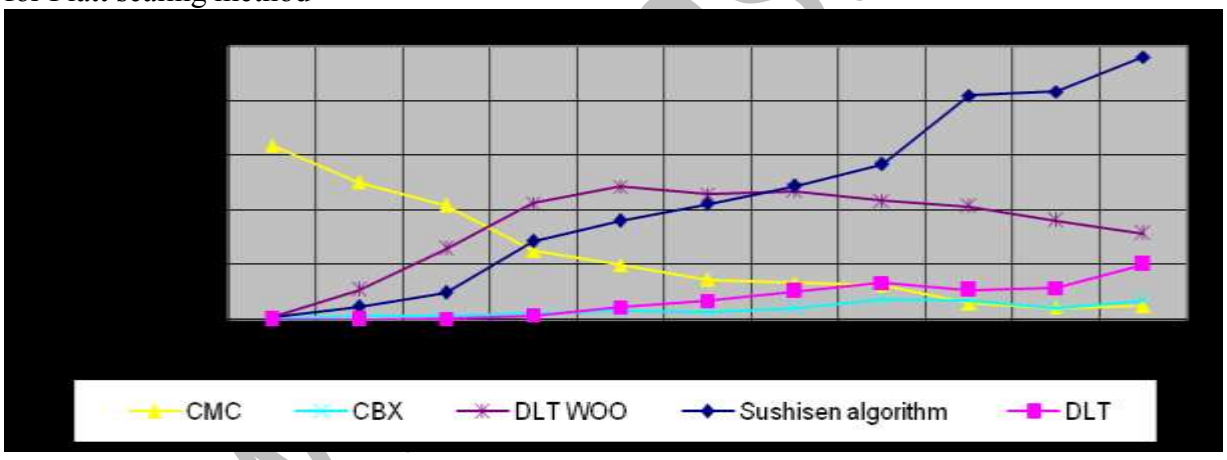


Fig:8 Over all image the final segmentation obtained methods with sushisen algorithm,

| Types | % AC | % PC | % FC | %C M | CT | RS | MF | TT | FR | LF | MM |
|---|---|---|---|---|---|---|---|---|---|---|---|
| CMC | 6,365 | 5,026 | 4,179 | 2,517 | 1,990 | 1,452 | 1,352 | 1,250 | 599 | 442 | 497 |
| CBX | 32 | 122 | 135 | 211 | 303 | 288 | 429 | 764 | 709 | 427 | 702 |
| DLT WOO | 69 | 1,090 | 2,585 | 4,254 | 4,868 | 4,573 | 4,686 | 4,333 | 4,127 | 3,622 | 3,157 |
| Sushisen algorithm | 87 | 478 | 983 | 2,865 | 3,609 | 4,219 | 4,884 | 5,683 | 8,188 | 8,334 | 9,591 |
| DLT | 0 | 0 | 21 | 159 | 454 | 687 | 1040 | 1356 | 1083 | 1167 | 2026 |

Table 1: New segmentation uncertainty estimation in terms of the accuracy of the final segmentation after DLT Methods fitting

## COMPARISON STUDY

TABLE 2: NIMA Comparison Study

| Classifier | Three data set Dataset | Number of Test Attributes | Correctly Classified Attributes | Classification rate (%) |
|---|---|---|---|---|
| Sushisen algorithm (proposed) | DLT WOO Dataset | 1200 | 1150 | 97.77 |
| | CBX.CMC Dataset | 1200 | 1160 | 97.77 |
| KNN | ABC Dataset | 1200 | 1020 | 85 |
| | PSO Dataset | 1200 | 980 | 81.67 |
| NP | PSO Data set | 1200 | 990 | 82,5 |
| | ABC Dataset | 1200 | 940 | 78.33 |

The performance of the Sushisen algorithms is better than KNN and NP. Table V explains the Comparison of algorithms - BABC, KNN and NP. Fig. 1 shows the performance analysis of the algorithms which Table V explains in a bar chat. Fig. 2 exhibits the performance analysis of the algorithms using Multidimensional to show the algorithm Sushisen is better than KNN and NP in extracting the details according to the user's need with better accuracy.

**a)System Description**

The Toshiba Portege R600 U2530 laptop is powered by Intel Core 2 Duo SU9400, 1400 Mega Hertz (Mhz) processor. This Portege series laptop from Toshiba comes with 3072 Megabytes (MB) of RAM, which is expandable up to Megabytes (MB). Toshiba Portege R600 U2530 laptop or notebook PC has a 128Solid State Drive Gigabytes (GB) hard disk capacity, and HDMI Port. The display of Toshiba Portege R600 U2530 is with 1280 x 800 pixels resolution. This Toshiba laptop has a battery life of hours and weighs around 1 kgs. Operation system Windows 10 running the MATLAB Software programming.

## CONCLUSION

In this study, we have proposed a method for detecting tuberculosis From lung radiograph Our focus is on building aspects for the personal manifestations of tuberculosis using cancer specified in DLT WOO .Most of the work existing in the field is based on construction Features to show formatting and layout information Lungs. But many CXR films overlap body structures are also distorted by acquisitions Noise goes to the wrong information Size and design details. Such features do not apply. The size is very large and is not well-normalized for others In the data set We tried to see the indirect effects of lungs on the lungs Abnormalities rather than directly analyzing the severity Change. The features are based on what points Radiologists see the X-ray image. We achieved great results Compared to the refined CMC working in the Indians Dataset But since no direct comparison is possible Dataset differences Our feature vector is almost the same Tenth part of the length of the description of the size and design Performance oriented TB detection system is analyzed Area of receiver working under (AUC) rules (ROC) curve For the removed section, we follow the following procedure Per column Retrieve index with non-zero values and all pixels and take it in column of the left and right lungs, respectively. Factors Calculate the

difference between two consecutive factors Each array to get the difference range And it stores the rib's width and Sushisen algorithm using constant lines in intervals In fact we really can not only remove the ribs with rows Distance is always different because each rib map is different Whether or not the rib space is attacked on odd lines We are not aware of the starting point. To estimate took one Each category of average is indicated 97.77% accuracy.

**REFERENCES**


i. Anas, E.M.A., Nouranian, S., Mahdavi, S.S., Spadinger, I., Morris, W.J., Salcudean, S.E., Mousavi, P., Abolmaesumi, P., 2017. Clinical target-volume delineation in prostate brachytherapy using residual neural networks. In: International Conference on Medical Image Computing and Computer-Assisted Intervention. Springer, pp. 365–373.

ii. Barra, V., Boire, J.-Y., 2001. Automatic segmentation of subcortical brain structures in mr images using information fusion. IEEE Trans. Med. Imag. 20 (7), 549–558.

iii. Betrouni, N., Vermandel, M., Pasquier, D., Maouche, S., Rousseau, J., 2005. Segmentation of abdominal ultrasound images of the prostate using a priori information and an adapted noise filter. Comput. Med. Imag. Graph. 29 (1), 43–51.

iv. Blake, A., Curwen, R., Zisserman, A., 1993. A framework for spatiotemporal control in the tracking of visual contours. Int. J. Comput. Vis. 11 (2), 127–145.

v. Choromanska, A., Henaff, M., Mathieu, M., Arous, G.B., LeCun, Y., 2015. The loss surfaces of multilayer networks. In: Artificial Intelligence and Statistics, pp. 192–204.

vi. Cootes, T.F., Taylor, C.J., Cooper, D.H., Graham, J., 1995. Active shape models-their training and application. Comput. Vis. Image Understand. 61 (1), 38–59.

vii. Elhamifar, E., Vidal, R., 2013. Sparse subspace clustering: algorithm, theory, and applications. IEEE Trans. Pattern Anal. Mach. Intell. 35 (11), 2765–2781.

viii. Gal, Y., 2016. Uncertainty in Deep Learning. University of Cambridge. Gal, Y., Ghahramani, Z., 2015. Bayesian convolutional neural networks with Bernoulli approximate variational inference. arXiv: 1506.02158.

ix. Ghavami, N., Hu, Y., Bonmati, E., Rodell, R., Gibson, E., Moore, C., Barratt, D., 2018. Integration of spatial information in convolutional neural networks for automatic segmentation of intraoperative transrectal ultrasound images. J. Med. Imag. 6

x. (1), 011003.

xi. Ghose, S., Oliver, A., Martí, R., Lladó, X., Vilanova, J.C., Freixenet, J., Mitra, J.,Sidibé, D., Meriaudeau, F., 2012. A survey of prostate segmentation methodologies in ultrasound, magnetic resonance and computed tomography images. Comput. Method. Progr. Biomed. 108 (1), 262–287.

xii. Ghose, S., Oliver, A., Mitra, J., Martí, R., Lladó, X., Freixenet, J., Sidibé, D., Vilanova, J.C., Comet, J., Meriaudeau, F., 2013. A supervised learning framework of statistical shape and probability priors for automatic prostate segmentation in ultrasound images. Med. Image Anal. 17 (6), 587–600.

xiii. Gibson, E., Hu, Y., Ghavami, N., Ahmed, H.U., Moore, C., Emberton, M., Huisman, H.J.,Barratt, D.C., 2018. Inter-site variability in prostate segmentation accuracy using Deep learning. In: International Conference on Medical Image Computing and Computer-Assisted Intervention. Springer, pp. 506–514.

xiv. Goodfellow, I., Bengio, Y., Courville, A., Bengio, Y., 2016. Deep Learning, 1. MIT press

xv. Cambridge. Guo, C., Pleiss, G., Sun, Y., Weinberger, K.Q., 2017. On calibration of modern neural networks. arXiv: 1706.04599.

xvi. Hodge, A.C., Fenster, A., Downey, D.B., Ladak, H.M., 2006. Prostate boundary segmentation from ultrasound images using 2d active shape models: optimisation and extension to 3d. Comput. Method. Progr. Biomed. 84 (2), 99–113.

xvii. Huang, G., Liu, Z., Weinberger, K.Q., van der Maaten, L., 2017. Densely connected convolutional networks. In: Proceedings of the IEEE Conference on Computer Vision and Pattern Recognition, 1, p. 3.

xviii. Jemal, A., Bray, F., Center, M.M., Ferlay, J., Ward, E., Forman, D., 2011. Global cancer statistics. CA: A Cancer J. Clin. 61 (2), 69–90.

xix. Jendoubi, A., Zeng, J., Chouikha, M.F., 2004. Segmentation of prostate ultrasound images using an improved snakes model. In: Signal Processing, 2004. Proceedings. ICSP'04. 2004 7th International Conference on, 3. IEEE, pp. 2568–2571.

xx. Ji, P., Zhang, T., Li, H., Salzmann, M., Reid, I., 2017. Deep subspace clustering networks. In: Advances in Neural Information Processing Systems, pp. 23–32.

xxi. Kachouie, N.N., Fieguth, P., Rahnamayan, S., 2006. An elliptical level set method for automatic TRUS prostate image segmentation. In: Signal Processing and Information Technology, 2006 IEEE International Symposium on. IEEE, pp. 191–196.

xxii. Karimi, D., Zeng, Q., Mathur, P., Avinash, A., Mahdavi, S., Spadinger, I., Abolmaesumi, P., Salcudean, S., 2018. Accurate and robust segmentation of the clinical target volume for prostate brachytherapy. In: Frangi, A.F., Schnabel, J.A., Davatzikos, C., Alberola-López, C., Fichtinger, G. (Eds.), Medical Image Computing and Computer Assisted Intervention – MICCAI 2018. Springer International Publishing, Cham, pp. 531–539.

xxiii. Kendall, A., Cipolla, R., 2016. Modelling uncertainty in deep learning for camera relocalization. In: 2016 IEEE International Conference on Robotics and Automation (ICRA). IEEE, pp. 4762–4769.

xxiv. Kendall, A., Gal, Y., 2017. What uncertainties do we need in Bayesian deep learning for computer vision? In: Advances in Neural Information Processing Systems, pp. 5574–5584.

xxv. Kingma, D.P., Ba, J., 2014. Adam: a method for stochastic optimization. In: Proceedings of the 3rd International Conference on Learning Representations (ICLR). Kohavi, R., Wolpert, D.H., et al., 1996. Bias plus variance decomposition for zero-one loss functions. ICML, 96. 275–83

xxvi. Kuncheva, L., Whitaker, C., 2003. Measures of diversity in classifier ensembles and their relationship with the ensemble accuracy. Mach. Learn. 51 (2), 181–207.

xxvii. Lakshminarayanan, B., Pritzel, A., Blundell, C., 2017. Simple and scalable predictive uncertainty estimation using deep ensembles. In: Advances in Neural Information Processing Systems, pp. 6402–6413.

xxviii. Li, X., Li, C., Fedorov, A., Kapur, T., Yang, X., 2016. Segmentation of prostate from ultrasound images using level sets on active band and intensity variation across edges. Med. Phys. 43 (6Part1), 3090–3103.

xxix. Mahdavi, S.S., Chng, N., Spadinger, I., Morris, W.J., Salcudean, S.E., 2011. Semi-automatic segmentation for prostate interventions. Med. Image Anal. 15 (2),226–237.

xxx. Milletari, F., Navab, N., Ahmadi, S.-A., 2016. V-net: fully convolutional neural networks for volumetric medical image segmentation. In: 3D Vision (3DV), 2016 Fourth International Conference on. IEEE, pp. 565–571.

xxxi. Morris, W.J., Keyes, M., Spadinger, I., Kwan, W., Liu, M., McKenzie, M., Pai, H., Pickles, T., Tyldesley, S., 2013. Population-based 10-year oncologic outcomes after low-dose-rate brachytherapy for low-risk and intermediate-risk prostate cancer. Cancer 119 (8), 1537–1546.

xxxii. Mozaffari, M.H., Lee, W., 2016. 3d ultrasound image segmentation: a survey. arXiv:

xxxiii. 1611.09811.

xxxiv. Naeini, M.P., Cooper, G.F., Hauskrecht, M., 2015. Obtaining well calibrated probabilities using Bayesian binning. In: AAAI, pp. 2901–2907.

xxxv. Nag, S., Bice, W., DeWyngaert, K., Prestidge, B., Stock, R., Yu, Y., 2000. The American brachytherapy society recommendations for permanent prostate brachytherapy postimplant dosimetric analysis. Int. J. Radiat. Oncol. Biol. Phys. 46 (1), 221–230.

xxxvi. Neal, R.M., 2012. Bayesian Learning for Neural Networks, 118. Springer Science & Business Media. Noble, J.A., Boukerroui, D., 2006. Ultrasound image segmentation: a survey. IEEE Trans. Med. Imag. 25 (8), 987–1010.

xxxvii. Nouranian, S., Mahdavi, S.S., Spadinger, I., Morris, W.J., Salcudean, S.E., Abolmaesumi, P., 2015. A multi-atlas-based segmentation framework for prostate brachytherapy. IEEE Trans. Med. Imag. 34 (4), 950–961.

xxxviii. Nouranian, S., Ramezani, M., Spadinger, I., Morris, W.J., Salcudean, S.E., Abolmaesumi, P., 2016. Learning-based multi-label segmentation of transrectal ultrasound images for prostate brachytherapy. IEEE Trans. Med. Imag. 35 (3), 921–932.

xxxix. Pawlowski, N., Brock, A., Lee, M.C., Rajchl, M., Glocker, B., 2017. Implicit weight uncertainty in neural networks. arXiv: 1711.01297.